ia617

Spin Contamination in Inorganic Chemistry Calculations

Jason L. Sonnenberg and H. Bernhard Schlegel

Wayne State University, Detroit, MI, USA

and

Hrant P. Hratchian

Gaussian Inc., Wallingford, CT, USA

1 INTRODUCTION

Advances in both theoretical methods and computer hardware over the past four decades have led to an ever-increasing synergy between experiments and electronic structure calculations. This is particularly apparent in the inorganic chemistry community where calculations are routinely employed to understand problems ranging from spectra deconvolution to bonding in relativistic actinoid complexes (*see* ***Computational Methods: Lanthanides and Actinides***). A wide variety of electronic structure methods currently exist to accurately describe closed-shell, ground-state singlet systems. Unfortunately, not all chemistry occurs on closed-shell, singlet potential energy surfaces so issues such as symmetry breaking in open-shell compounds must be addressed.

From the theorems of linear Hermitian operators, it is known that a common and complete set of eigenfunctions exists for two operators, $\boldsymbol{A}$ and $\boldsymbol{B}$, that commute, i.e., $[\boldsymbol{A}, \boldsymbol{B}] = 0$.[1] Therefore, the set of eigenfunctions for a nonrelativistic Hamiltonian, $\boldsymbol{H}$, should also be eigenfunctions of the spin operator, $\boldsymbol{S}^2$, and the spatial symmetry operators ($\boldsymbol{E}, \boldsymbol{C}_n, \boldsymbol{\sigma}, \boldsymbol{i}$, etc.) for the relevant nuclear point group because these operators commute with $\boldsymbol{H}$. Spin symmetry breaking occurs when the eigenstates are not eigenfunctions of $\boldsymbol{S}^2$. In such cases, Ψ_0 is said to be *spin contaminated* owing to incorporation of higher spin state character as evidenced by expectation values of $\boldsymbol{S}^2$, $\langle \boldsymbol{S}^2 \rangle$, larger than $S(S+1)$.[2,3] If the resulting eigenstates are not eigenfunctions of the symmetry operations for the full nuclear point group, then Ψ_0 exhibits spatial symmetry breaking and is dubbed a *broken-symmetry* wave function.[4] Although broken-symmetry wave functions do not exhibit all the expected eigenvalue properties, they are not without use (*see* ***Broken Symmetry States of Iron–Sulfur Clusters***). It is important to note that while spin-contaminated and broken-symmetry wave functions are related, one does not beget the other.

Löwdin pointed out that the computational chemist is faced with a symmetry dilemma requiring a balance to

Computational Inorganic and Bioinorganic Chemistry. Edited by Edward I. Solomon, Robert A. Scott and R. Bruce King.
 ISBN 978-0-470-69997-3

be struck between imposing constraints to enforce correct spin-symmetry properties in the resulting eigenfunctions or increasing the variational parameters to achieve the lowest energy.[5] Restricting each occupied orbital in a closed-shell system to contain one α and one β electron is the simplest way to enforce spin symmetry, $\langle \boldsymbol{S}^2 \rangle = 0$, and results in the restricted family of methods denoted by an R prefixed to the method's acronym (e.g., RHF, RMP2, RB3LYP, etc.). For open-shell systems, spin symmetry is preserved when each unpaired electron resides in an α spin orbital with the remaining electrons constrained to doubly occupied orbitals thereby defining the restricted open-shell methodologies denoted by an RO in beginning of a method's acronym. Although RO methods preserve spin symmetry and increase the variational parameters compared to restricted methods, practical experience has shown that they do not provide adequate structures, energies, and spin densities.[6] Beyond RO methods, multiconfiguration self-consistent field (MCSCF), single and multireference (MR) configuration interaction (CI) methods utilizing spin-adapted configuration state functions (CSFs) maximize the variational flexibility within a truncated CI framework while providing spin contamination-free wave functions. Unfortunately, MCSCF, single-reference CI, and multireference configuration interaction (MRCI) methods are all too frequently impractical for systems of interest. Returning to a single-determinant framework, the variational flexibility can be increased beyond RO methods by allowing different orbitals for different spins (DODS). These so-called unrestricted methods are indicated with a U prefixed to the method's standard acronym (e.g., UHF, UMP2, UB3LYP, etc.) and the resulting eigenstates are no longer eigenfunctions of $\boldsymbol{S}^2$. The variational flexibility in a single-determinant method is maximized when each electron is described as a linear combination of α and β spin orbitals. Such generalized methods are denoted with a G prefixed to the method's acronym and generate eigenstates that are not eigenfunctions of $\boldsymbol{S}^2$. Understanding how to navigate Löwdin's symmetry dilemma of balancing flexibility versus constraints via practical application of the aforementioned classes of methods is the focus of the rest of this article. Readers not interested in a rigorous development of the underlying mathematical principles may wish to skip ahead to Sections 5 or 6.

2 HARTREE–FOCK

Since many correlated methods, including hybrid density functional theory (DFT), build upon Hartree–Fock (HF) theory, it is reviewed here to illustrate the mathematical underpinnings behind spin contamination. Interested readers should see Jensen[2] or other standard texts for a more detailed derivation of the HF equations.[7] The electronic wave function for an N-electron system is denoted by a normalized Slater determinant, Ψ_0, containing N spin orbitals ψ_i.

$$\Psi_0 = |\psi_1 \psi_2 \ldots \psi_N\rangle \tag{1}$$

Following the variational principle, the spin orbitals are optimized to minimize the energy, E, while maintaining a normalized total wave function.

$$E = \langle \Psi_0 | \mathbf{H} | \Psi_0 \rangle \tag{2}$$

In equation (2), $\boldsymbol{H}$ is the full electronic Hamiltonian after application of the Born–Oppenheimer approximation. Minimizing E with respect to ψ_i under the constraint of orthonormality, the following one-electron eigenvalue equations emerge:

$$\mathbf{F}_i \psi_i = \varepsilon_i \psi_i \tag{3}$$

F_i is the effective one-electron Fock operator for the ith electron given by

$$\mathbf{F}_i = \boldsymbol{h}_i + \boldsymbol{V}_i^{\mathrm{HF}} \tag{4}$$

where $\boldsymbol{h}_i$ is also a one-electron operator describing the motion of electron i in the electric field generated by N_{nuclei} each with charge Z_A

$$\boldsymbol{h}_i = -\frac{1}{2}\boldsymbol{\Delta}_i^2 - \sum_A^{N_{\mathrm{nuclei}}} \frac{Z_A}{\mathbf{r}_{iA}} \tag{5}$$

and $\boldsymbol{V}_i^{\mathrm{HF}}$ is the mean field potential experienced by electron i owing to the presence of the other electrons.

$$\boldsymbol{V}_i^{\mathrm{HF}} = \sum_j^N \boldsymbol{J}_j - \boldsymbol{K}_j \tag{6}$$

$$\boldsymbol{J}_j |\psi_i(1)\rangle = \langle \psi_j(2) | \frac{1}{\mathbf{r}_{12}} | \psi_j(2) \rangle |\psi_i(1)\rangle \tag{7}$$

$$\boldsymbol{K}_j |\psi_i(1)\rangle = \langle \psi_j(2) | \frac{1}{\mathbf{r}_{12}} | \psi_i(2) \rangle |\psi_j(1)\rangle \tag{8}$$

Following the method of Roothaan[8] and Hall,[9] the spatial part, ϕ_i, of each spin orbital can be written as a linear combination of M basis functions, χ_ν

$$\psi_i = \varphi_i(\mathbf{r}) = \sum_\nu^{M_{\mathrm{basis}}} C_{\nu i} \chi_\nu(\mathbf{r}) \tag{9}$$

Inserting equation (9) into equation (3) yields

$$\sum_\nu^{M_{\mathrm{basis}}} \boldsymbol{F}_i \chi_\nu C_{\nu i} = \varepsilon_i \sum_\nu^{M_{\mathrm{basis}}} \chi_\nu C_{\nu i} \tag{10}$$

which can be left multiplied by χ_μ and integrated to give

$$\sum_{\nu}^{M_{\text{basis}}} \left\{ F_{\mu\nu} - \varepsilon_i S_{\mu\nu} \right\} C_{\nu i} = 0 \quad i = 1, 2, \ldots, N \tag{11}$$

where $F_{\mu\nu} = \langle \chi_\mu | \boldsymbol{F} | \chi_\nu \rangle$ and $S_{\mu\nu} = \langle \chi_\mu | \chi_\nu \rangle$. Equation (11) can be further simplified by noting that **F** and **S** are $M_{\text{basis}} \times M_{\text{basis}}$ matrices, **C** is an $M_{\text{basis}} \times N$ matrix, and $\boldsymbol{\varepsilon}$ is a diagonal $N \times N$ matrix.

$$\mathbf{FC} = \mathbf{SC}\boldsymbol{\varepsilon} \tag{12}$$

F is the matrix formulation of the Fock operator, **C** is the matrix of molecular orbital (MO) coefficients, **S** is the overlap matrix between basis functions, and $\boldsymbol{\varepsilon}$ is a diagonal matrix of MO energies. Equation (12) is solved in an iterative manner beginning with an initial guess for **C** from which **F** is built. **F** is then used to generate a new **C** and the cycle is repeated until the change in energies converges below a numeric threshold and self-consistency is achieved. It is important to note that **F** is *nonlinear* in the MO coefficients because **J** and **K** in **F** depend upon **C**. Thus from a mathematical perspective, spin contamination is a direct manifestation of the nonlinearity of Fock operators.

Having reviewed the necessary HF equations, the differences between the R (restricted), RO (restricted open shell), U (unrestricted), and G (generalized) classes of methods are easy to see in terms of their corresponding orthonormal spin orbitals, ψ_i. In both restricted Hartree–Fock (RHF) and restricted open-shell Hartree–Fock (ROHF) theory, α and β spin orbitals have the same spatial functions and therefore identical values for $C_{\nu i}$. The coefficients can be real or complex and the wave functions are eigenfunctions of both $\boldsymbol{S}_z$ and $\boldsymbol{S}^2$.

$$\psi_i^\alpha(\mathbf{r}) = \varphi_i(\mathbf{r})\alpha, \quad \psi_i^\beta(\mathbf{r}) = \varphi_i(\mathbf{r})\beta, \quad \varphi_i(\mathbf{r}) = \sum_{\nu}^{M_{\text{basis}}} C_{\nu i}\chi_\nu(\mathbf{r}) \tag{13}$$

Unrestricted Hartree–Fock (UHF) theory uses spin orbitals in which α and β electrons may have different MO coefficients thereby resulting in different α and β spatial functions.

$$\begin{aligned} \psi_i^\alpha(\mathbf{r}) &= \varphi_{ia}^\alpha = \varphi_{ia}(\mathbf{r})\alpha = \left[\sum_{\nu}^{M_{\text{basis}}} C_{\nu i}^a \chi_\nu(\mathbf{r}) \right] \alpha, \\ \psi_i^\beta(\mathbf{r}) &= \varphi_{ib}^\beta = \varphi_{ib}(\mathbf{r})\beta = \left[\sum_{\nu}^{M_{\text{basis}}} C_{\nu i}^b \chi_\nu(\mathbf{r}) \right] \beta \end{aligned} \tag{14}$$

The UHF values of $C_{\nu i}^a$ and $C_{\nu i}^b$ can be either real or complex and the resulting wave functions are eigenfunctions of $\boldsymbol{S}_z$ but not $\boldsymbol{S}^2$. A generalized Hartree–Fock (GHF) spin orbital (also known as *generalized spin orbital* (*GSO*) in the literature) can also have real or complex MO coefficients, but now each spin orbital is a linear combination of both α and β spin orbitals.[10]

$$\begin{aligned} \psi_i(\mathbf{r}) &= \varphi_{ia}^\alpha + \varphi_{ib}^\beta = \varphi_{ia}(\mathbf{r})\alpha + \varphi_{ib}(\mathbf{r})\beta \\ &= \sum_{\nu}^{M_{\text{basis}}} \left\{ \left[C_{\nu i}^a \chi_\nu(\mathbf{r}) \right] \alpha + \left[C_{\nu i}^b \chi_\nu(\mathbf{r}) \right] \beta \right\} \end{aligned} \tag{15}$$

Although generalized spin orbitals have the most variational flexibility, they are not eigenfunctions of either $\boldsymbol{S}_z$ or $\boldsymbol{S}^2$.

3 SPIN OPERATORS

Computation of $\langle \boldsymbol{S}^2 \rangle$ is best understood in the framework of raising and lowering operators.[11] Let $\boldsymbol{S}_x$, $\boldsymbol{S}_y$, and $\boldsymbol{S}_z$ be the components of $\boldsymbol{S}$ along the denoted Cartesian axis. Raising, $\boldsymbol{S}_+$, and lowering, $\boldsymbol{S}_-$, operators for electronic spin are defined as follows:

$$\boldsymbol{S}_+ = \boldsymbol{S}_x + i\boldsymbol{S}_y, \quad \boldsymbol{S}_- = \boldsymbol{S}_x - i\boldsymbol{S}_y \tag{16}$$

$\boldsymbol{S}^2$ can now be expressed in atomic units for one electron in the following way:

$$\boldsymbol{S}^2 = \boldsymbol{S}_x^2 + \boldsymbol{S}_y^2 + \boldsymbol{S}_z^2 = \tfrac{1}{2}\left(\boldsymbol{S}_+\boldsymbol{S}_- + \boldsymbol{S}_-\boldsymbol{S}_+\right) + \boldsymbol{S}_z^2 \tag{17}$$

For many-electron systems, $\boldsymbol{S}^2$ takes the following form:

$$\begin{aligned} \boldsymbol{S}^2 = \frac{1}{2} &\left\{ \sum_{ij}^{N} \left[\boldsymbol{s}_+(i)\boldsymbol{s}_-(j) + \boldsymbol{s}_-(i)\boldsymbol{s}_+(j) \right] \right\} \\ &+ \left(\sum_{i}^{N} \boldsymbol{s}_z(i) \right) \left(\sum_{j}^{N} \boldsymbol{s}_z(j) \right) \end{aligned} \tag{18}$$

where lowercase letters indicate one-electron operators with the following properties in the α and β spin orbital basis sets:

$$\begin{aligned} \boldsymbol{s}_+\psi_i &= \boldsymbol{s}_+\varphi_{ia}^\alpha + \boldsymbol{s}_+\varphi_{ib}^\beta = \varphi_{ib}^\alpha \\ \boldsymbol{s}_-\psi_i &= \boldsymbol{s}_-\varphi_{ia}^\alpha + \boldsymbol{s}_-\varphi_{ib}^\beta = \varphi_{ia}^\beta \\ \boldsymbol{s}_x\psi_i &= \boldsymbol{s}_x\varphi_{ia}^\alpha + \boldsymbol{s}_x\varphi_{ib}^\beta = \frac{1}{2}\varphi_{ia}^\beta + \frac{1}{2}\varphi_{ib}^\alpha \\ \boldsymbol{s}_y\psi_i &= \boldsymbol{s}_y\varphi_{ia}^\alpha + \boldsymbol{s}_y\varphi_{ib}^\beta = \frac{i}{2}\varphi_{ia}^\beta - \frac{i}{2}\varphi_{ib}^\alpha \\ \boldsymbol{s}_z\psi_i &= \boldsymbol{s}_z\varphi_{ia}^\alpha + \boldsymbol{s}_z\varphi_{ib}^\beta = \frac{1}{2}\varphi_{ia}^\alpha - \frac{1}{2}\varphi_{ib}^\beta \end{aligned} \tag{19}$$

Using equation (19), the following molecular spin-expectation values can be derived:

$$\langle \boldsymbol{S}_+ \rangle = \sum_{i}^{N_{\text{occ}}} \mathcal{S}_{ii}^{ab}, \quad \langle \boldsymbol{S}_- \rangle = \sum_{i}^{N_{\text{occ}}} \mathcal{S}_{ii}^{ba}$$

$$\langle \boldsymbol{S}_+\boldsymbol{S}_-\rangle = \sum_i^{N_{\text{occ}}} \mathcal{S}_{ii}^{aa} + \langle \boldsymbol{S}_x\rangle^2 + \langle \boldsymbol{S}_y\rangle^2 - \sum_{ij}^{N_{\text{occ}}} \left|\mathcal{S}_{ij}^{ab}\right|^2$$

$$\langle \boldsymbol{S}_-\boldsymbol{S}_+\rangle = \sum_i^{N_{\text{occ}}} \mathcal{S}_{ii}^{bb} + \langle \boldsymbol{S}_x\rangle^2 + \langle \boldsymbol{S}_y\rangle^2 - \sum_{ij}^{N_{\text{occ}}} \left|\mathcal{S}_{ij}^{ab}\right|^2$$

$$\langle \boldsymbol{S}_x\rangle = \frac{1}{2}\sum_i^{N_{\text{occ}}} \left(\mathcal{S}_{ii}^{ba} + \mathcal{S}_{ii}^{ab}\right), \quad \langle \boldsymbol{S}_y\rangle = \frac{i}{2}\sum_i^{N_{\text{occ}}} \left(\mathcal{S}_{ii}^{ba} - \mathcal{S}_{ii}^{ab}\right)$$

$$\langle \boldsymbol{S}_z\rangle = \frac{1}{2}\sum_i^{N_{\text{occ}}} \left(\mathcal{S}_{ii}^{aa} - \mathcal{S}_{ii}^{bb}\right),$$

$$\langle \boldsymbol{S}_z^2\rangle = \frac{N_{\text{elec}}}{4} + \langle \boldsymbol{S}_z\rangle^2 - \frac{1}{4}\sum_{ij}^{N_{\text{occ}}} \left|\mathcal{S}_{ij}^{aa} - \mathcal{S}_{ij}^{bb}\right|^2 \tag{20}$$

The $\mathcal{S}_{ij}^{aa}$, $\mathcal{S}_{ij}^{bb}$, $\mathcal{S}_{ij}^{ab}$ and $\mathcal{S}_{ij}^{ba}$ terms are spatial orbital overlap integrals

$$\mathcal{S}_{ij}^{aa} = \langle \varphi_{ia}|\varphi_{ja}\rangle = \sum_{\mu\nu}^{M_{\text{basis}}} C_{\mu i}^{\text{a}^*} C_{\nu j}^{a} S_{\mu\nu},$$

$$\mathcal{S}_{ij}^{bb} = \langle \varphi_{ib}|\varphi_{jb}\rangle = \sum_{\mu\nu}^{M_{\text{basis}}} C_{\mu i}^{\text{b}^*} C_{\nu j}^{b} S_{\mu\nu}$$

$$\mathcal{S}_{ij}^{ab} = \langle \varphi_{ia}|\varphi_{jb}\rangle = \sum_{\mu\nu}^{M_{\text{basis}}} C_{\mu i}^{\text{a}^*} C_{\nu j}^{b} S_{\mu\nu},$$

$$\mathcal{S}_{ij}^{ba} = \langle \varphi_{ib}|\varphi_{ja}\rangle = \sum_{\mu\nu}^{M_{\text{basis}}} C_{\mu i}^{\text{b}^*} C_{\nu j}^{a} S_{\mu\nu} \tag{21}$$

resulting from the expectation-value integration step. Substituting the relations from equation (20) into equation (17) and recalling that $\sum_{i=1}^{N_{\text{occ}}} \left(\mathcal{S}_{ii}^{aa} + \mathcal{S}_{ii}^{bb}\right) = N_{\text{elec}}$, produces the general formula for $\langle \boldsymbol{S}^2\rangle$,

$$\begin{aligned}\langle \boldsymbol{S}^2\rangle &= \frac{1}{2}\left(\langle \boldsymbol{S}_+\boldsymbol{S}_-\rangle + \langle \boldsymbol{S}_-\boldsymbol{S}_+\rangle\right) + \langle \boldsymbol{S}_z^2\rangle \\ &= \frac{3}{4}N_{\text{elec}} + \langle \boldsymbol{S}_x\rangle^2 + \langle \boldsymbol{S}_y\rangle^2 + \langle \boldsymbol{S}_z\rangle^2 \\ &\quad - \sum_{ij}^{N_{\text{occ}}} |\mathcal{S}_{ji}^{ab}|^2 - \frac{1}{4}\sum_{ij}^{N_{\text{occ}}} |\mathcal{S}_{ij}^{aa} - \mathcal{S}_{ij}^{bb}|^2\end{aligned} \tag{22}$$

For unrestricted spin orbitals, $\mathcal{S}_{ij}^{aa} = \delta_{ij}$ when i and j are α orbital indices; otherwise, $\mathcal{S}_{ij}^{aa}$ equals zero. Similarly, $\mathcal{S}_{ij}^{bb} = \delta_{ij}$ when i and j are β orbital indices; otherwise, $\mathcal{S}_{ij}^{bb}$ equals zero. Therefore, $\langle \boldsymbol{S}^2\rangle$ reduces to

$$\begin{aligned}\langle \boldsymbol{S}^2\rangle_{\text{U}} &= \frac{3}{4}N_{\text{elec}} + \langle \boldsymbol{S}_z\rangle^2 - \sum_{ij}^{N_{\text{occ}}} \left|\mathcal{S}_{ji}^{ab}\right|^2 - \frac{1}{4}N_{\text{elec}} \\ &= \langle \boldsymbol{S}_z\rangle\left(\langle \boldsymbol{S}_z\rangle + 1\right) + n_\beta - \sum_{ij}^{N_{\text{occ}}} \left|\mathcal{S}_{ji}^{ab}\right|^2\end{aligned} \tag{23}$$

For restricted spin orbitals, $\mathcal{S}_{ij}^{ab} = \mathcal{S}_{ij}^{ba} = \delta_{ij}$, and $\langle \boldsymbol{S}^2\rangle_{\text{U}}$ collapses to

$$\langle \boldsymbol{S}^2\rangle_{\text{R}} = \langle \boldsymbol{S}_z\rangle\left(\langle \boldsymbol{S}_z\rangle + 1\right), \quad \langle \boldsymbol{S}_z\rangle = \frac{1}{2}(n_\alpha - n_\beta) \tag{24}$$

For unrestricted spin orbitals, a unitary transformation among the occupied orbitals can be made such that the $\mathcal{S}^{ab}$ matrix is diagonal. The resulting rotated orbitals are termed *corresponding orbitals* and their use greatly simplifies the matrix element expressions for $\boldsymbol{S}^{2n}$.[12–14]

Møller–Plesset (MPn) perturbation theory is a convenient implementation of many-body perturbation theories (MBPTn), which adds correlation corrections to HF wave functions. For second-order Møller–Plesset perturbation theory (MP2) calculations, $\langle \boldsymbol{S}^2\rangle$ is given by

$$\langle \boldsymbol{S}^2\rangle = \langle \Psi_0|\boldsymbol{S}^2|\Psi_0\rangle + 2\langle \Psi_0|\boldsymbol{S}^2|\Psi_1\rangle \tag{25}$$

where $|\Psi_1\rangle$ is the first-order correction to the HF wave function. Expressions for higher-order MPn theory have been worked out, but quickly become complicated.[15] When computing $\langle \boldsymbol{S}^2\rangle$ for correlated methods such as configuration interaction with doubles (CID), configuration interaction with singles and doubles (CISD), quadratic configuration interaction with singles and doubles (QCISD), coupled-cluster theory, and Brueckner doubles (BD), a perturbation, $\lambda\boldsymbol{S}^2$, is added to $\boldsymbol{H}$ so that $\boldsymbol{S}^2$ can be computed as a derivative.[16–18]

Since density functional theory (DFT) does not formally employ a wave function, correctly calculating $\langle \boldsymbol{S}^2\rangle$ becomes challenging. If equation (22) is used with the occupied Kohn–Sham orbitals, the resulting value of $\langle \boldsymbol{S}^2\rangle$ is very close to S(S + 1), but this value is for the *noninteracting* system rather than for the true interacting system of interest.[19,20] Multireference density functional theory (MR-DFT),[21,22] in which CSFs are constructed using some DFT matrix elements or constrained density functional theory with configuration interaction (CDFT-CI)[23] may provide improved $\langle \boldsymbol{S}^2\rangle$ values. Since $\boldsymbol{S}^2$ is a two-particle property, its expectation value can be computed from the two-particle density matrix. For single-determinant methods, the two-particle density matrix can be expressed in terms of one-particle density matrices and correlation hole functions.[19] Unfortunately, the exact one-particle density matrix is only known for the exchange-only uniform electron gas, thus *all* DFT $\langle \boldsymbol{S}^2\rangle$ values are approximate.

4 PROJECTION OPERATORS

Unwanted spin states can be removed from spin-contaminated wave functions with Löwdin's spin projection

operators[24] derived from the properties of Hermitian spaces[25]:

$$\boldsymbol{P}_s = \prod_{k \neq s} \frac{\boldsymbol{S}^2 - k(k+1)}{s(s+1) - k(k+1)} \tag{26}$$

Since $|\Psi_0\rangle$ can be expanded into a basis set of pure spin states, $|\Phi_i\rangle$,[26,27]

$$|\Psi_0\rangle^{2S+1} = \sum_{i=S} C_i |\Phi_i\rangle \tag{27}$$

full application of the projection operators sets all but the first coefficient in equation (27) to zero. Projection operators for removing spins $s+1$ to $s+n$ involve operators $\boldsymbol{S}^2$ through $\boldsymbol{S}^{2n}$. Truncation of $\boldsymbol{P}_s$ after the first term produces the annihilation operator for removing only the state with spin k from $|\Psi_0\rangle$.

$$\boldsymbol{A}_k = \frac{\boldsymbol{S}^2 - k(k+1)}{\langle \boldsymbol{S}^2 \rangle - k(k+1)} \tag{28}$$

Besides removing all spin k components, $\boldsymbol{A}_k$ also changes the relative weighting of the remaining spin components.[28] The projection operator is idempotent, $\boldsymbol{P}_s{}^2 = \boldsymbol{P}_s$, but for annihilation operators this is not the case.[13] Projection or annihilation can be incorporated into the self-consistent field (SCF) procedure since both operators commute with spin-free Hamiltonians. It is important to note that application of either projection or annihilation operators after the SCF procedure produces wave functions that are *no longer stationary* with respect to the variational parameters. Practical experience has shown that spin contamination often occurs from only a few spin states such that $\boldsymbol{P}_s$ is well approximated by one or two annihilators.[29]

5 PROJECTED METHODS

Inclusion of the full projection operator into HF theory leads to the so-called extended Hartree–Fock (EHF) method.[30] Given the complexity of the EHF equations and the fact that only RHF or ROHF wave functions are eigenfunctions of $\boldsymbol{S}^2$,[31] approximate projection methods are most commonly utilized. The interested reader is referred to previous reviews of these methods for a historical perspective.[30,32]

The projected energy of a previously determined UHF wave function can be evaluated as an expectation value.

$$E_{\mathrm{PUHF}} = \frac{\langle \boldsymbol{P}_s \Psi_0 | \boldsymbol{H} | \boldsymbol{P}_s \Psi_0 \rangle}{\langle \boldsymbol{P}_s \Psi_0 | \boldsymbol{P}_s \Psi_0 \rangle} = \frac{\langle \Psi_0 | \boldsymbol{H} \boldsymbol{P}_s | \Psi_0 \rangle}{\langle \Psi_0 | \boldsymbol{P}_s | \Psi_0 \rangle} = E_{\mathrm{UHF}} + \Delta E_{\mathrm{PUHF}} \tag{29}$$

If more than one higher spin state contributes significantly to the spin contamination, then approximating $\boldsymbol{P}_s$ with a single annihilator can result in projected energies that are artificially lower than the fully projected energy and not size-consistent.[28,33] Although inclusion of a sufficient number of annihilators will remove the artificial energy lowering,[34,35] it does not eliminate the discontinuity found in bond-dissociation curves at the RHF → UHF instability (see Figure 1). Therefore, projected unrestricted Hartree–Fock (PUHF) theory is *not* recommended for computing reaction energetics or exploring potential energy surfaces even though analytic PUHF gradients[36] were worked out. Likewise, projected-DFT is generally *not* recommended for radicals and dissociation potentials because projection degrades the unrestricted DFT results beyond the RHF/UHF instability point.[37]

The total MPn energy can be expressed as an expectation value with the following form:

$$E_{\mathrm{MP}n} = \langle \Psi_0 | \boldsymbol{H} | \Psi_0 + \Psi_1 + \cdots \Psi_{n-1} \rangle \tag{30}$$

Application of projection operators to the MPn wave function proceeds in a manner similar to HF theory.[15,29,38]

$$E_{\mathrm{proj\,MP}n} = \frac{\langle \Psi_0 | \boldsymbol{H} \boldsymbol{P}_s | \Psi_0 + \Psi_1 + \cdots \Psi_{n-1} \rangle}{\langle \Psi_0 | \boldsymbol{P}_s | \Psi_0 + \Psi_1 + \cdots \Psi_{n-1} \rangle} \tag{31}$$

and when expanded order by order, results in the same projected energy expression as applying the projection while developing the perturbation series.[34] If the perturbative corrections for electron correlation, $\Psi_1 + \cdots \Psi_{n-1}$, are Schmidt orthogonalized to the PUHF wave function, then an approximate formula for projected Møller–Plesset perturbation theory (PMPn) energy is obtained.[29,38] This approximate formula and the corresponding analytic gradients work quite well for projected second-order Møller–Plesset perturbation theory (PMP2) compared to equation (31) and are much simpler to implement.[36] In the case of PMP2, the energy expression is given by

$$E_{\mathrm{PMP2}} = E_{\mathrm{MP2}} + \Delta E_{\mathrm{PUHF}} \left(1 - \frac{\langle \Psi_1 | \tilde{\Psi}_0 \rangle}{\langle \tilde{\Psi}_0 | \tilde{\Psi}_0 \rangle} \right)$$
$$P_s \Psi_0 = \Psi_0 + \tilde{\Psi}_0 \tag{32}$$

Since unrestricted Møller–Plesset perturbation theory (UMPn) energies can be substantially higher than their projected counterparts, the use of spin-projected UMPn energies is generally recommended.

Alternatives to projected UMPn include various open-shell spin-restricted perturbation approaches, such as open-shell perturbation theory method 1 (OPT1), open-shell perturbation theory method 2 (OPT2), restricted Møller–Plesset perturbation theory (RMPn, also known as *restricted open-shell Hartree–Fock many-body perturbation theory*, *ROHF-MBPTn*), restricted open-shell Møller–Plesset perturbation theory (ROMPn), and Z-averaged perturbation

theory (ZAPTn). Since OPT1 and OPT2 employ eigenfunctions of $\boldsymbol{S}^2$ in the perturbation expansion, the resulting energies are free of spin contamination. However, the perturbation series is susceptible to convergence and rotational invariance difficulties.[39] RMPn, ROMPn, and ZAPTn methods use a restricted open-shell reference determinant, but some spin contamination enters via the perturbation expansion. Differences between these methods are usually small. ZAPTn tends to be a bit better for difficult cases and provides significant computational advantages because it uses the same spatial parts for the α and β spin orbitals.[40]

It was shown that operation of any single annihilator, $\boldsymbol{A}_{k+n}$, upon the coupled cluster singles and doubles (CCSD) wave function leaves the CCSD energy unchanged [38]. Similar behavior, in which some degree of projection is naturally included in the method, is found for QCISD, and BD energies.[15,38,41] Because of this, spin-unrestricted QCISD, coupled cluster (CC), and BD methods are less affected by spin contamination and are normally employed without projection. Spin-adapted coupled-cluster methods have been developed and are spin contamination-free.[42]

In situations where the spin contamination is small, Yamaguchi and coworkers devised an approximate projection (AP) method that does not explicitly require annihilation operators.[43] The AP method connects the concepts of projection operators to spin Hamiltonians. Although all of the aforementioned methods with the exception of EHF are approximate projection techniques, the AP abbreviation has become associated with only Yamaguchi's approach in the literature. When spin contamination is small, $\boldsymbol{P}_s$ is accurately approximated by $\boldsymbol{A}_k$ and equation (27) can be written as

$$|\Psi_0\rangle^{2S+1} = C_S|\Phi_S\rangle + C_{S+1}|\Phi_{S+1}\rangle \tag{33}$$

where S and S + 1 denote the pure low-spin state with multiplicity 2S + 1 and high-spin state with multiplicity 2S + 3 respectively. The expectation values of energy and $\boldsymbol{S}^2$ take the following form since the pure spin states are orthonormal:

$$E_0 = C_S^2 E_S + C_{S+1}^2 E_{S+1} = (1 - C_{S+1}^2)E_S + C_{S+1}^2 E_{S+1} \tag{34}$$

$$\begin{aligned}\langle \boldsymbol{S}^2\rangle_0 &= (1 - C_{S+1}^2)\langle \boldsymbol{S}^2\rangle_S + C_{S+1}^2\langle \boldsymbol{S}^2\rangle_{S+1} \\ &= \langle \boldsymbol{S}^2\rangle_S + C_{S+1}^2\left(\langle \boldsymbol{S}^2\rangle_{S+1} - \langle \boldsymbol{S}^2\rangle_S\right)\end{aligned} \tag{35}$$

From equation (35) the high-spin state coefficient can be calculated as

$$C_{S+1}^2 = \frac{\langle \boldsymbol{S}^2\rangle_0 - \langle \boldsymbol{S}^2\rangle_S}{\langle \boldsymbol{S}^2\rangle_{S+1} - \langle \boldsymbol{S}^2\rangle_S} = \frac{\langle \boldsymbol{S}^2\rangle_0 - S(S+1)}{2(S+1)} \tag{36}$$

If the high-spin wave function with a multiplicity of 2S + 3 computed at the low-spin geometry, $|\Psi_0\rangle^{2S+3}$, *does not have any significant* spin contamination, then it is a good approximation for $|\Phi\rangle_{S+1}$ and $\langle \boldsymbol{S}^2\rangle_{S+1} \approx \langle \boldsymbol{S}^2\rangle_0^{2S+3}$. Solving equation (34) for E_S with these approximations yields

$$E_S = \alpha E_0 - \beta E_{S+1} \approx \alpha E_0 - \beta E_0^{2S+3} \tag{37}$$

The coefficients in the preceding equation take the following forms

$$\begin{aligned}\alpha &= \frac{1}{1 - C_{S+1}^2} \\ &= \frac{\langle \boldsymbol{S}^2\rangle_{S+1} - \langle \boldsymbol{S}^2\rangle_S}{\langle \boldsymbol{S}^2\rangle_{S+1} - \langle \boldsymbol{S}^2\rangle_0} \approx \frac{\langle \boldsymbol{S}^2\rangle_0^{2S+3} - \langle \boldsymbol{S}^2\rangle_S}{\langle \boldsymbol{S}^2\rangle_0^{2S+3} - \langle \boldsymbol{S}^2\rangle_0}, \quad \beta = 1 - \alpha\end{aligned} \tag{38}$$

Gradients were worked out so that geometry optimizations can be carried out for any level of theory for which $\langle \boldsymbol{S}^2\rangle$ can be calculated.[44] The AP method is closely related to Ziegler's method for determining multiplet energies, which is also based upon equation (33) and determines the coefficients from group theory.[45,46] It is important to note that if $|\Psi_0\rangle^{2S+3}$ is spin contaminated, then methods based upon equation (33) may fail or require recursive application.

6 APPLICATIONS

Spin contamination can become an especially difficult issue for structures exhibiting strained bonds, such as transition structures, as well as for studies of (multi-) radical chemistry. To simulate bond strain and radical formation, bond-dissociation curves for H_2 and ScH are examined to demonstrate some of the concepts outlined above. The former allows us to illustrate essential physics within the context of a well-understood and chemically intuitive process, while the latter provides a practical example where factors common to transition metal chemistry, in particular, can complicate electronic structure calculations. The discussion is presented in qualitative terms, but readers seeking thorough mathematical details are referred to an earlier review where the bond dissociation of H_2 is also considered.[32] All calculations were carried out using the development version of the Gaussian suite of electronic structure programs.[47]

6.1 H_2 Case Study

Energy versus H–H bond length curves are plotted in Figure 1(a). These curves are the three potential energy surfaces available for H_2 with the STO-3G[48] minimal basis set in which one s orbital is centered on each H atom. Electronic structure descriptions of these states can be understood using MO theory. At short bond distances, the two 1s atomic orbitals (AOs) combine to form bonding and antibonding MOs. At these distances, the RHF singlet wave function properly generates the ground-state MO configuration as $1\sigma_g^2$. At very

long distances the two 1s AOs do not overlap, remain localized on their respective atomic center, and are degenerate. The RHF singlet wave function now incorrectly leads to a solution that includes character from the ionic product $H^+ + H^-$. The correct H + H product state is given by the triplet description; however, at short bond distances, the triplet state leads to a $1\sigma_g{}^1 1\sigma_g{}^{*1}$ electronic configuration and a bond order of zero.

Figure 1(b) shows the lowest eigenvalues of the RHF orbital-rotation Hessian, or stability matrix,[49,50] and the singlet UHF $\langle \boldsymbol{S}^2 \rangle$ as functions of the H–H distance. Where the lowest orbital-rotation Hessian eigenvalue is negative, the RHF wave function is unstable and a UHF wave function is lower in energy. At bond distances less than ~1.2 Å, the triplet state is significantly higher in energy than the singlet state, and the UHF (singlet) and RHF wave functions are the same. Thus, the RHF wave function is stable in this region and the singlet UHF $\langle \boldsymbol{S}^2 \rangle$ is zero. For bond distances greater than ~1.2 Å, the RHF wave function is not stable and the singlet UHF energy is lowest. At long distances, the singlet UHF wave function localizes one electron on each atomic center. To achieve this electronic structure within a single-determinantal picture requires the UHF singlet wave function to break spin symmetry by mixing with the pure UHF triplet state thereby resulting in spin contamination. The degree of triplet contamination is a maximum at long distances where the UHF singlet $\langle \boldsymbol{S}^2 \rangle = 1$, indicating equal mixing of pure singlet and triplet states.

Figure 2 displays energy profiles for H_2 evaluated using various wave function methods, including full CI. An important effect of spin contamination is the inclusion of static correlation (also known as *left–right correlation* or *nondynamic correlation*)[51] by mixing in triplet and excited singlet states. As a result, employing projection operators to remove spin contamination from the UHF singlet state yields an unphysical dissociation curve. The PUHF energy profile suffers from a cusp and an unphysical local minimum near the RHF → UHF instability.

When correlation corrections are explicitly included, using second-order Møller–Plesset perturbation theory with an RHF reference (RMP2) for example, an artificial energy maximum is observed at 2.4 Å and at long bond lengths, the energy heads to $-\infty$ as the energy denominator goes to zero. Using second-order Møller–Plesset perturbation theory with a UHF reference (UMP2) yields a curve that approaches the correct limit. Despite the fact that perturbation theory captures a large proportion of electron correlation, it is not able to remove higher spin states from the reference wave function. This deficiency leads to poor convergence in the MP

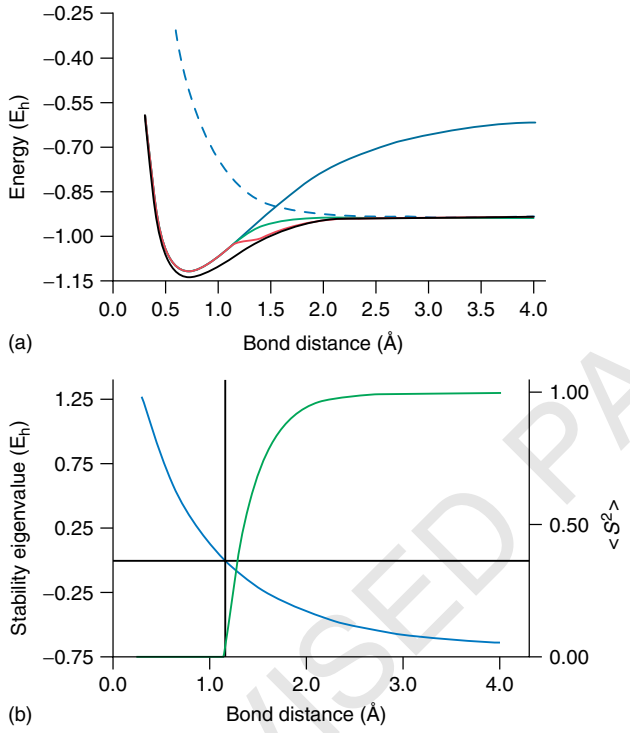

Figure 1 (a) Full CI (——), RHF singlet (——), UHF singlet (——), PUHF singlet (——), and UHF triplet (– – –) energy profiles; and (b) the lowest RHF singlet orbital-rotation Hessian eigenvalue (——) and $\langle \boldsymbol{S}^2 \rangle$ for the UHF singlet wave function (——) plotted against the H_2 bond length. Black horizontal and vertical lines denote a stability eigenvalue of 0 and the bond distance where the RHF → UHF instability onset is observed, respectively

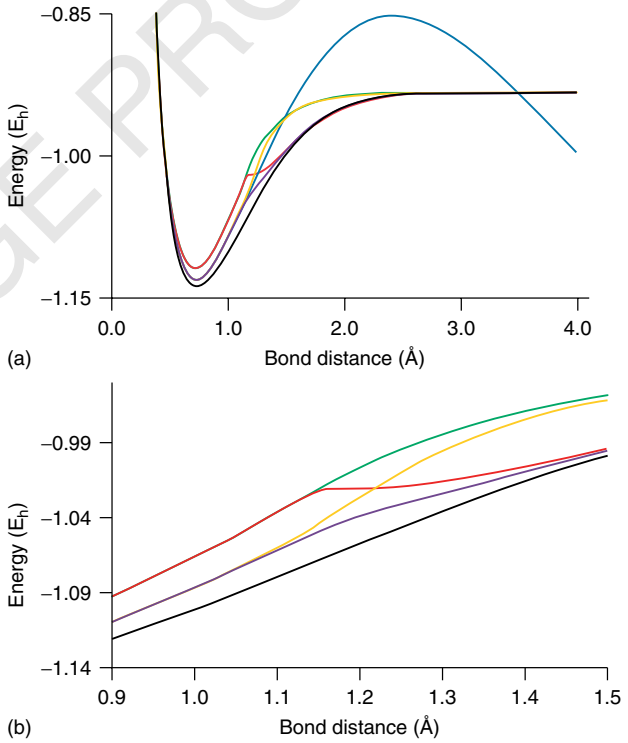

Figure 2 (a) Energy profiles for Full CI (——), UHF (——), PUHF (——), RMP2 (——), UMP2 (——), and unrestricted PMP2 (——) plotted against H_2 the bond length; and (b) an enlarged view of the Full CI, UHF, PUHF, UMP2, and unrestricted PMP2 energy profiles

series for cases displaying significant spin contamination.[52–55] Spin projection can correct this problem and lead to very good performance, particularly in the region just beyond the instability point where the unrestricted PMP2 (using equation 32) dissociation curve is comparable to the full CI result (Figure 2).

Because dynamic correlation contributions are included at a computational cost that scales the same as HF, DFT has become the workhorse of computational inorganic chemistry.[56] While DFT is not a panacea, it does perform quite well in many routine studies including cases where spin contamination presents difficulties for wave function methods. As mentioned above, the evaluation of DFT $\langle \boldsymbol{S}^2 \rangle$ values is not necessarily straightforward. Some time ago, Becke and coworkers showed that computing $\langle \boldsymbol{S}^2 \rangle$ for the interacting system—which requires the two-particle density—yields results that are typically larger than for the noninteracting system.[19] Note that the true, and as yet unknown, density functional would provide a proper $\boldsymbol{S}^2$ eigenstate with a $\langle \boldsymbol{S}^2 \rangle$ value equal to S(S + 1). For computational simplicity, we use the noninteracting system to compute $\langle \boldsymbol{S}^2 \rangle$ for DFT examples discussed here.

Figure 3 presents $\langle \boldsymbol{S}^2 \rangle$ and the lowest eigenvalue of the restricted-DFT stability matrices as functions of the H–H bond distance using the BLYP[57,58] pure functional and the B3LYP[59] hybrid functional. Also included in Figure 3 are data from the B2PLYP double-hybrid functional, which incorporates virtual orbital dependencies through the inclusion of an MP2 energy correction term.[60] The general behavior of these curves is similar to the UHF curves described previously. However, onset of the restricted → unrestricted instability for all three DFT models comes later in the dissociation curve than for HF. While $\langle \boldsymbol{S}^2 \rangle$ and stability curves for these DFT levels are nearly the same, onset of the restricted → unrestricted instability is earliest for B2PLYP, followed by B3LYP, and BLYP. This ordering is likely due to the extent of HF exchange included in the functional definitions (53% for B2PLYP, 20% for B3LYP, and 0% for BLYP). Likewise, the lowest stability matrix eigenvalue grows more negative more slowly for BLYP than for B3LYP or B2PLYP.

Energy profiles for H_2 dissociation using BLYP, B3LYP, and B2PLYP functionals are shown in Figure 4. In general, it is seen that the restricted and unrestricted DFT curves differ from one another analogous to the qualitative differences between RHF and UHF energy profiles (Figure 1a). Prior to the restricted → unrestricted instability both R and U curves are the same for BLYP and B3LYP. After the instability point, restricted and unrestricted profiles differ. While the unrestricted curves lead to an asymptotic limit that is quite

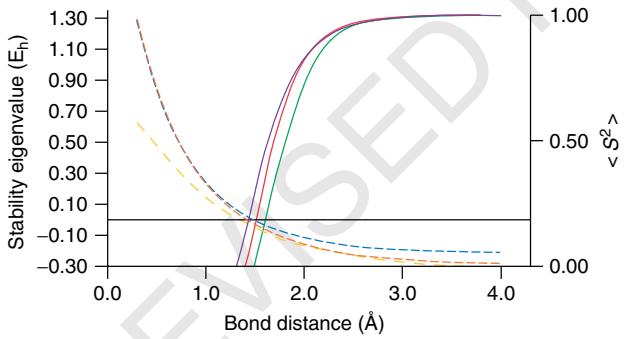

Figure 3 Lowest RBLYP (– – –), RB3LYP (– – –), and RB2PLYP (– – –) orbital-rotation Hessian eigenvalues, and $\langle \boldsymbol{S}^2 \rangle$ for UBLYP (——), UB3LYP (——), and UB2PLYP (——) wave function plotted against the H_2 bond length

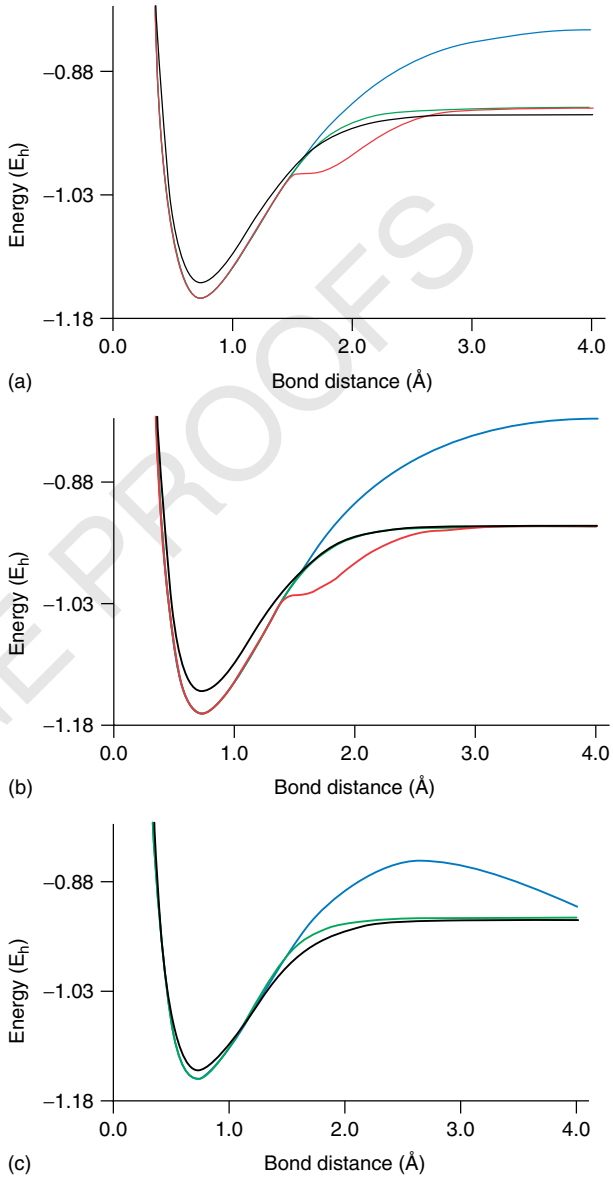

Figure 4 (a) RBLYP (——), UBLYP (——), PUBLYP (——); (b) RB3LYP (——), UB3LYP (——), PUB3LYP (——); and (c) RB2PLYP (——) and UB2PLYP (——) energy curves plotted against the H_2 bond length. As a reference, the Full CI (——) energy curve appears in all plots

close to the full CI result, RBLYP and RB3LYP energies have large differences relative to full CI at large H–H distances. The UBLYP and UB3LYP profiles agree much better with the full CI curve. In the same manner as UHF, unrestricted DFT solutions are capable of including static correlation by allowing the different spatial components of α and β MOs, which gives broken spin-symmetry Kohn–Sham densities beyond the restricted → unrestricted instability point. Projection techniques can also be applied to DFT in the same way as is done for PUHF where the Kohn–Sham orbitals are used to construct excited determinants and the spin projector is approximated by a single annihilator using only doubles excitations.[37,61] Projection of the spin contaminant in the UBLYP and UB3LYP calculations leads to the same unphysical energy profiles as the PUHF results in Figure 2. Therefore, use of projected-DFT is *not* a recommended method.[37]

The behavior of the B2PLYP double-hybrid functional is quite similar to MP2 (Figure 2). RB2PLYP incorrectly displays a large energy barrier at 2.7 Å after which the energy leads to $-\infty$. Note that the RB2PLYP barrier appears later than the RMP2 barrier at 2.4 Å. The UB2PLYP energy profile does lead to the correct dissociation limit, and qualitatively gives the correct shape of the potential energy curve. Again, this observation is analogous to the behavior of UMP2. Figure 4(c) also includes the dissociation curve given by the SCF energy of the UB2PLYP reference determinant, and it is seen that the post-SCF correction changes the H_2 dissociation curve by a small amount, which is consistent with the fact that this double-hybrid functional includes only 27% of the second-order perturbation energy. The use of projection techniques with double-hybrid functionals has not yet been fully studied, though initial tests measuring thermodynamics indicate that spin projection may not be necessary in these cases.[62] These early results seem reasonable given that Kohn–Sham determinants tend to suffer less from spin contamination and that only a fraction of post-SCF contributions are included in these energy expressions. Nevertheless, the utility of projection methods in the context of double-hybrid DFT functionals may require further consideration.

6.2 ScH Case Study

Many inorganic systems, especially transition metal complexes, can suffer from spin contamination problems in a manner analogous to elongated H_2. For recent examples, see Refs. 63 and 64 along with works cited therein. Often multiple spin states contribute to the contamination, and the standard approach of annihilating the first, $s + 1$, spin contaminant may not be adequate. As an example of such cases, we now consider the bond dissociation of ScH on the $^1\Sigma$ electronic ground state. All calculations were carried out using the 6-31G(d) basis set.[65] Figure 5(a) shows RHF, UHF (singlet), and PUHF ScH dissociation curves; the lowest eigenvalue of the RHF orbital-rotation Hessian is shown together with the UHF $\langle \hat{S}^2 \rangle$ in Figure 5(b).

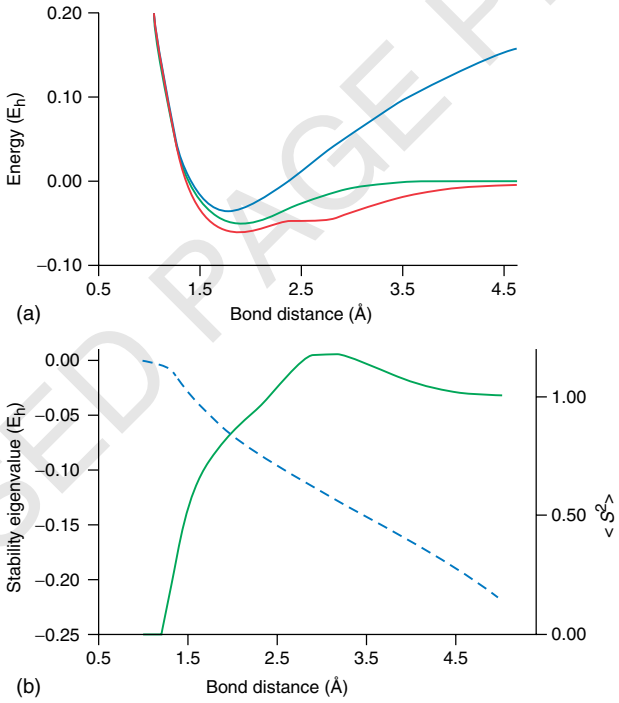

Figure 5 (a) RHF (——), UHF (——), and projected-UHF (——) energy profiles; and (b) the lowest RHF singlet orbital-rotation Hessian eigenvalue (– – –) and $\langle \hat{S}^2 \rangle$ for the UHF singlet wave function (——) plotted against the ScH bond length

The plots included in Figure 5 show some interesting behaviors. First, unlike H_2, onset of the RHF → UHF instability is quite early for ScH. Whereas the H_2 RHF wave function is stable for some distance beyond the energy minimum, RHF → UHF instability begins at Sc–H bond lengths shorter than the energy minimum. As a result, RHF and UHF models predict two different equilibrium bond lengths. As seen in Figure 5(b), the UHF solution displays a significant amount of spin contamination beyond 1.1 Å. At the dissociation limit, $\langle \boldsymbol{S}^2 \rangle$ goes to 1.0, which is consistent with a broken-symmetry, open-shell singlet state similar to the solution of H_2 at long bond lengths. However, for ScH, $\langle \boldsymbol{S}^2 \rangle$ does not trace out a monotonic or sigmoid curve as in the H_2 case. Instead, between the onset of the RHF → UHF instability and complete dissociation, the UHF solution is contaminated by higher spin states causing $\langle \boldsymbol{S}^2 \rangle$ to grow beyond 1.0 for a significant portion of the dissociation process.

Figure 6 shows the energy profiles using the MP2 level of theory. Unfortunately, a full CI calculation on this system is not feasible and direct comparison of MP2 and CI dissociation curves is not available. Nevertheless, the RMP2 curve is certainly incorrect and the UMP2 curve shows an unphysical maximum to dissociation.

As seen in the previous example, applying projection methods does not yield a satisfactory result in the case of PUHF (Figure 5a). Similar to the H_2 results studied earlier, the PUHF curve presents a second local energy minimum and displays an unphysical approach to the dissociation limit. Interestingly, the unrestricted PMP2 curve is much less acceptable than the UMP2 profile. The unrestricted PMP2 energy profile is unphysical and resembles the PUHF curve more than the UMP2 curve. This result is due to contaminants in the reference UHF wave function with spin multiplicities higher than 3. Recall from Section 5 that the usual approximation in the unrestricted PMP2 energy expression is that only the next higher spin state contaminates the UHF reference wave function. Removing the triplet contaminant with a single annihilator operator reweights the relative contamination of higher states,[32] and, in this case, leads to a severe distortion of the unrestricted PMP2 dissociation curve beginning around 2.5 Å, which is also where the UHF $\langle \boldsymbol{S}^2 \rangle$ rises above 1.0.

With more computational expense, it is possible to annihilate additional spin contaminants. Energy profiles using unrestricted PMP2 with two and three contaminants projected are also shown in Figure 6. Projection of two contaminants essentially corrects the unrestricted PMP2 curve and gives a correct physical picture of bond dissociation. The third projection is probably not needed, as is demonstrated by the fact that curves with two and three projected contaminants are indistinguishable. More quantitatively, one can evaluate the $\langle \boldsymbol{S}^2 \rangle$ values as successive projections are applied. At a bond length of 2.5 Å, $\langle \boldsymbol{S}^2 \rangle$ values for the reference wave function with one, two, three, and four projections are 0.715, 0.001, 0.000, and 0.000. At a bond length of 3.1 Å, where the unprojected UHF $\langle \boldsymbol{S}^2 \rangle$ is at its maximum of 1.184, $\langle \boldsymbol{S}^2 \rangle$ values for the projected reference wave functions are 1.328, 0.002, 0.000, and 0.000.

Figure 7 shows energy profiles and $\langle \boldsymbol{S}^2 \rangle$ curves for ScH dissociation using UBLYP, UB3LYP, and UB2PLYP. The energy profiles predict much larger bond energies than MP2, though the depth of the minimum decreases going from BLYP to B3LYP to B2PLYP as contributions from

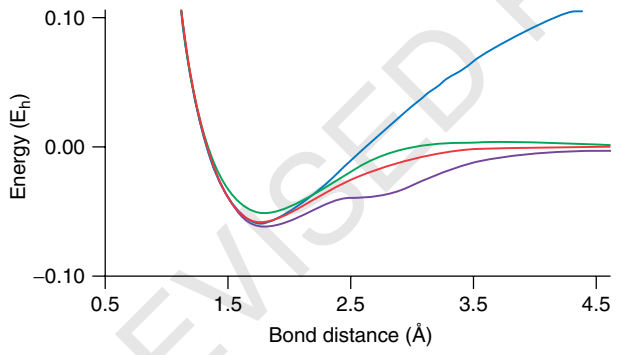

Figure 6 (a) Energy profiles for RMP2 (——), UMP2 (——), UMP2 with one spin projection (——), UMP2 with two spin projections (——), and UMP2 with three spin projections (——) plotted against the ScH bond length

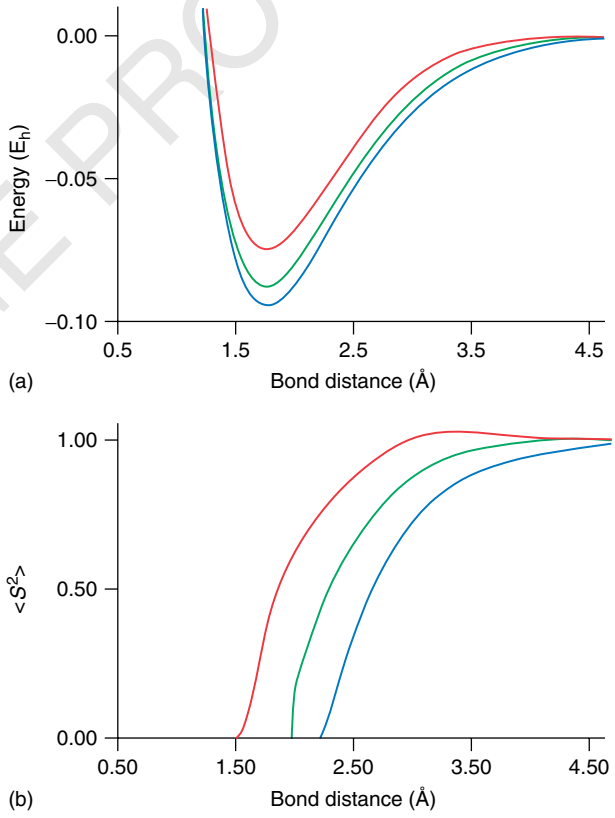

Figure 7 (a) UBLYP (——), UB3LYP (——), and UB2PLYP (——) energy profiles; and (b) $\langle \boldsymbol{S}^2 \rangle$ for UBLYP, UB3LYP, and UB2PLYP singlet determinants plotted against the ScH bond length

HF exchange and explicit dynamic correlation are included. More central to the topic of interest here are the $\langle \boldsymbol{S}^2 \rangle$ curves given in Figure 7(b). In all three cases, the DFT $\langle \boldsymbol{S}^2 \rangle$ values approach 1.0 at long bond distance indicating equal admixture of pure singlet and triplet states in the unrestricted DFT Kohn–Sham determinants, which is similar to the observed UHF behavior in Figure 5(b). However, the DFT results suggest much less contamination from higher spin states. In fact, B3LYP and BLYP $\langle \boldsymbol{S}^2 \rangle$ curves do not appear to have any significant contaminants higher than triplet states. As seen in the H_2 example, the onset of spin contamination for the DFT determinants comes later in the ScH curve than for the HF wave function. For B3LYP and BLYP, spin contamination does not become problematic until after the energy minimum. The B2PLYP determinant does begin to show spin contamination near the minimum, possibly because of the much higher percentage of HF exchange. Another important difference between DFT and HF is the range of bond distances over which $\langle \boldsymbol{S}^2 \rangle$ rises from 0.0 to 1.0, which is the range where the consequences of spin contamination are most severe. Note that DFT methods move quickly from the pure singlet state to the mixed open-shell singlet configuration.

This example demonstrates three important aspects of spin contamination in computational inorganic chemistry. First, in cases where restricted wave functions at optimized geometries are not stable, nonnegligible geometric changes may accompany relaxation of the wave function constraints. For ScH, relaxing the RHF wave function by using the broken spin-symmetry UHF solution at the RHF optimized geometry decreases the absolute energy by more than $35\,\mathrm{kJ\,mol^{-1}}$. Reoptimizing the geometry using the UHF wave function leads to an increase in the bond distance of 0.11 Å and a $40\,\mathrm{kJ\,mol^{-1}}$ decrease in absolute energy. Note, though, that the spin-contaminated UHF minimum geometry does not differ too much from the geometry on the spin-projected MP2 surface. As mentioned in the literature, spin contamination is a marker of energy errors, with highly contaminated wave functions yielding energy errors on the order of $40-50\,\mathrm{kJ\,mol^{-1}}$; however, the effect of spin contamination on geometry is much less predictable.[36] Second, it is common for more than one spin contaminant to affect the quality of HF wave functions. While most systems display a small, if not negligible, degree of contamination from $s+1$ and higher spin states, it is not atypical for transition metal systems to display significant contamination by $s+2$ and possibly higher spin states. In these cases, the most common and computationally economic choice of annihilating only the $s+1$ contaminant may yield worse results than using a spin-contaminated solution. Third, it was seen that DFT models contend better with spin contamination than HF. This is not to say that DFT determinants are free of spin contamination, but even for the extreme case of ScH, BLYP and B3LYP functionals include contamination only from $s+1$ states. Moreover, the range of the potential energy surface affected by spin contamination—the region where $\langle \boldsymbol{S}^2 \rangle$ rises from 0.0 to 1.0—is much smaller than in the HF case. We have also seen that the recently developed double-hybrid density functionals perform quite well for ScH bond dissociation, although future studies are certainly necessary to fully understand the scope of applicability of these new functionals.

7 CONCLUSION

In summary, spin contamination occurs when a system's wave function or density incorporates character from higher spin states thereby resulting in $\langle \boldsymbol{S}^2 \rangle$ values larger than $s(s+1)$. The formulas necessary for determining these spin operator expectation values were developed for use with generalized, unrestricted, and restricted spin orbitals. Although these formulas are exact for wave functions, the corresponding equations for modern exchange-correlation functionals are an area ripe for future efforts. Current projection techniques were reviewed for a variety of wave function and density functional methods. As the ScH example clearly illustrates, spin contamination is an issue that all chemists performing computational experiments must be mindful of, particularly when metals are present in the system of interest.

8 ACKNOWLEDGMENTS

The authors thank Drs. Ken Dyall (Schrödinger Inc.), Michael Frisch (Gaussian, Inc.), and Artëm Masunov (University of Central Florida), along with Mr. Nicholas Mayhall (Indiana University) for helpful discussions and preprints.

9 RELATED ARTICLES

Ab initio and Semiempirical Methods; Broken Symmetry States of Iron–Sulfur Clusters; Computational Methods: Lanthanides and Actinides; Determining Transition States in Bioinorganic Reactions; Approximate Density Functionals: Which Should I Choose?; Electronic Strucutre of Metal–Metal Bonds; Multiconfigurational Quantum Mechanics (QM) for Heavy Element Compounds; Potential Energy Surfaces for Metal-Assisted Chemical Reactions; Spin-Orbit Coupling: Effects in Heavy Element Chemistry; Theoretical Aspects of Main Group Multiple Bonded Systems. ia611 ia618 ia640 ia609 ia615 ia631 ia614 ia639 ia655 ia662

10 ABBREVIATIONS AND ACRONYMS

AP = approximate projection; AO = atomic orbital; au = atomic units; BD = Brueckner doubles; CDFT-CI = constrained density functional theory with configuration interaction; CI = configuration interaction; CID = configuration interaction with doubles; CISD = configuration interaction with singles and doubles; CSF = configuration state function; DFT = density functional theory; DODS = different orbitals for different spins; E_h = Hartree energy units; EHF = extended Hartree–Fock; G = generalized; GHF = generalized Hartree–Fock; GSO = generalized spin orbital; HF = Hartree–Fock; MCSCF = multiconfiguration self-consistent field; MBPT*n* = many-body perturbation theory; MO = molecular orbital; MP*n* = Møller–Plesset perturbation theory; MR = multireference; MRCI = multireference configuration interaction; MR-DFT = multireference density functional theory; OPT1 = open-shell perturbation theory method 1; OPT2 = open-shell perturbation theory method 2; PUHF = projected unrestricted Hartree–Fock; PMP*n* = projected Møller–Plesset perturbation theory; QCI = quadratic configuration interaction; QCISD = quadratic configuration interaction with singles and doubles; R = restricted; RHF = restricted Hartree–Fock; RMP*n* = restricted Møller–Plesset perturbation theory; RO = restricted open-shell; ROHF-MBPT*n* = restricted open-shell Hartree–Fock many-body perturbation theory; ROMP*n* = restricted open-shell Møller–Plesset perturbation theory; SCF = self- consistent field; U = unrestricted; UHF = unrestricted Hartree–Fock; UMP*n* = unrestricted Møller–Plesset perturbation theory; ZAPT*n* = *Z*-averaged perturbation theory.

11 REFERENCES

1. I. N. Levine, 'Quantum Chemistry', 5th edition, Prentice-Hall, Inc., New Jersey, 2000.
2. F. Jensen, 'Introduction to Computational Chemistry', 2nd edition, John Wiley & Sons Inc., New Jersey, 2007.
3. C. J. Cramer, 'Essentials of Computational Chemistry', John Wiley & Sons Inc., New York, 2002.
4. H. Fukutome, *Int. J. Quantum Chem.*, 1981, **20**, 955.
5. P. Lykos and G. W. Pratt, *Rev. Mod. Phys.*, 1963, **35**, 496.
6. Y.-Y. Chuang, E. L. Coitiño, and D. G. Truhlar, *J. Phys. Chem. A*, 2000, **104**, 446.
7. S. Attila and N. S. Ostlund, 'Modern Quantum Chemistry', Dover Publications, Mineola, NY, 1996.
8. C. C. J. Roothaan, *Rev. Mod. Phys.*, 1951, **23**, 69.
9. G. G. Hall, *Proc. R. Soc. London*, 1951, **A205**, 541.
10. P.-O. Löwdin and I. Mayer, *Adv. Quantum Chem.*, 1992, **24**, 79.
11. J. J. Sakurai, 'Modern Quantum Mechanics', Revised edition, Addison-Wesley Publishing Company, Inc., New York, 1994.
12. A. T. Amos and G. C. Hall, *Proc. Roy. Soc. London*, 1961, **263**, 483.
13. T. Amos and L. C. Snyder, *J. Chem. Phys.*, 1964, **41**, 1773.
14. J. E. Harriman, *J. Chem. Phys.*, 1964, **40**, 2827.
15. W. Chen and H. B. Schlegel, *J. Chem. Phys.*, 1994, **101**, 5957.
16. J. F. Stanton, *J. Chem. Phys.*, 1994, **101**, 371.
17. H. Sekino and R. J. Bartlett, *J. Chem. Phys.*, 1985, **82**, 4225.
18. G. D. Purvis III, H. Sekino, and R. J. Bartlett, *Collect. Czech. Chem. Commun.*, 1988, **53**, 2203.
19. J. Wang, A. D. Becke, and V. H. Smith Jr, *J. Chem. Phys.*, 1995, **102**, 3477.
20. A. J. Cohen, D. J. Tozer, and N. C. Handy, *J. Chem. Phys.*, 2007, **126**, 214104.
21. S. Grimme and M. Waletzke, *J. Chem. Phys.*, 1999, **111**, 5645.
22. E. V. Beck, E. A. Stahlberg, L. W. Burggraf, and J.-P. Blaudeau, *Chem. Phys.*, 2008, **349**, 158.
23. Q. Wu, C.-L. Cheng, and T. Van Voorhis, *J. Chem. Phys.*, 2007, **127**, 164119.
24. P.-O. Löwdin, *Phys. Rev.*, 1955, **97**, 1509.
25. P. Cassam-Chenaï, *Int. J. Quantum Chem.*, 1998, **68**, 91.
26. F. Sasaki and K. Ohno, *J. Math. Phys.*, 1963, **4**, 1140.
27. S. Thanos and A. K. Theophilou, *J. Chem. Phys.*, 2006, **124**, 204109.
28. E. R. Davidson and A. E. Clark, *Int. J. Quantum Chem.*, 2005, **103**, 1.
29. H. B. Schlegel, *J. Chem. Phys.*, 1986, **84**, 4530.
30. I. Mayer, *Adv. Quantum Chem.*, 1980, **12**, 189.
31. P. Cassam-Chenaï and G. S. Chandler, *Int. J. Quantum Chem.*, 1993, **46**, 593.
32. H. B. Schlegel, in 'Encyclopedia of Computational Chemistry', eds. P. v.R. Schleyer, N. L. Allinger, T. Clark, J. Gasteiger, P. A. Kollman, H. F. Schaefer and P. R. Schreiner, John Wiley & Sons, New York, 1998, Vol. 4.
33. N. Koga, K. Yamashita, and K. Morokuma, *Chem. Phys. Lett.*, 1991, **184**, 359.
34. P. J. Knowles and N. C. Handy, *J. Phys. Chem.*, 1988, **92**, 3097.
35. P. J. Knowles and N. C. Handy, *J. Chem. Phys.*, 1988, **88**, 6991.
36. J. J. W. McDouall and H. B. Schlegel, *J. Chem. Phys.*, 1989, **90**, 2363.
37. J. M. Wittbrodt and H. B. Schlegel, *J. Chem. Phys.*, 1996, **105**, 6574.
38. H. B. Schlegel, *J. Phys. Chem.*, 1988, **92**, 3075.
39. T. J. Lee, A. P. Rendell, K. G. Dyall, and D. Jayatilaka, *J. Chem. Phys.*, 1994, **100**, 7400.
40. S. E. Wheeler, A. D. Wesley, and H. F. Schaefer III, *J. Chem. Phys.*, 2008, **128**, 74107.
41. H. Yuan and D. Cremer, *Chem. Phys. Lett.*, 2000, **324**, 389.
42. X. Li and J. Paldus, *Int. J. Quantum Chem.*, 2000, **77**, 281.

43. K. Yamaguchi, F. Jensen, A. Dorigo, and K. N. Houk, *Chem. Phys. Lett.*, 1988, **149**, 537.
44. Y. Kitagawa, T. Saito, M. Ito, M. Shoji, K. Koizumi, S. Yamanaka, T. Kawakami, M. Okumura, and K. Yamaguchi, *Chem. Phys. Lett.*, 2007, **442**, 445.
45. T. Ziegler, A. Rauk, and E. J. Baerends, *Theor. Chim. Acta (Berl.)*, 1977, **43**, 261.
46. C. Daul, *Int. J. Quantum Chem.*, 1994, **52**, 867.
47. M. J. Frisch, G. W. Trucks, H. B. Schlegel, G. E. Scuseria, M. A. Robb, J. R. Cheeseman, J. A. Montgomery Jr, T. Vreven, G. Scalmani, B. Mennucci, V. Barone, G. A. Petersson, M. Caricato, H. Nakatsuji, M. Hada, M. Ehara, K. Toyota, R. Fukuda, J. Hasegawa, M. Ishida, T. Nakajima, Y. Honda, O. Kitao, H. Nakai, X. Li, H. P. Hratchian, J. E. Peralta, A. F. Izmaylov, K. N. Kudin, J. J. Heyd, E. Brothers, V. Staroverov, G. Zheng, R. Kobayashi, J. Normand, J. L. Sonnenberg, F. Ogliaro, M. Bearpark, P. V. Parandekar, G. A. Ferguson, N. J. Mayhall, S. S. Iyengar, J. Tomasi, M. Cossi, N. Rega, J. C. Burant, J. M. Millam, M. Klene, J. E. Knox, J. B. Cross, V. Bakken, C. Adamo, J. Jaramillo, R. Gomperts, R. E. Stratmann, O. Yazyev, A. J. Austin, R. Cammi, C. Pomelli, J. W. Ochterski, P. Y. Ayala, K. Morokuma, G. A. Voth, P. Salvador, J. J. Dannenberg, V. G. Zakrzewski, S. Dapprich, A. D. Daniels, M. C. Strain, O. Farkas, D. K. Malick, A. D. Rabuck, K. Raghavachari, J. B. Foresman, J. V. Ortiz, Q. Cui, A. G. Baboul, S. Clifford, J. Cioslowski, B. B. Stefanov, G. Liu, A. Liashenko, P. Piskorz, I. Komaromi, R. L. Martin, D. J. Fox, T. Keith, M. A. Al-Laham, C. Y. Peng, A. Nanayakkara, M. Challacombe, W. Chen, M. W. Wong, J. A. Pople, Revision G.03 ed., 'The Development Version of the Gaussian Suite', Gaussian, Inc., Wallingford, CT, 2008.
48. W. J. Hehre, R. F. Stewart, and J. A. Pople, *J. Chem. Phys.*, 1969, **51**, 2657.
49. R. Seeger and J. A. Pople, *J. Chem. Phys.*, 1977, **66**, 3045.
50. H. B. Schlegel and J. J. W. McDouall, in 'Computational Advances in Organic Chemistry: Molecular Structure and Reactivity', eds. C. Ogretir and I. G. Csizmadia, Kluwer Academic Publishers, Boston, 1991, Vol. 330 p. 167.
51. K. Raghavachari and J. B. Anderson, *J. Phys. Chem.*, 1996, **100**, 12960.
52. N. C. Handy, P. J. Knowles, and K. Somasundram, *Theoret. Chim. Acta (Berl.)*, 1985, **68**, 87.
53. P. W. Gill and L. Radom, *Chem. Phys. Lett.*, 1986, **132**, 16.
54. R. H. Nobes, J. A. Pople, L. Radom, N. C. Handy, and P. J. Knowles, *Chem. Phys. Lett.*, 1987, **138**, 481.
55. M. W. Wong and L. Radom, *J. Phys. Chem.*, 1995, **99**, 8582.
56. S. Niu and M. B. Hall, *Chem. Rev.*, 2000, **100**, 353.
57. A. D. Becke, *Phys. Rev. A*, 1988, **38**, 3098.
58. C. Lee, W. Yang, and R. G. Parr, *Phys. Rev. B*, 1988, **37**, 785.
59. P. J. Stephens, F. J. Devlin, C. F. Chabalowski, and M. J. Frisch, *J. Phys. Chem.*, 1994, **98**, 11623.
60. S. Grimme, *J. Chem. Phys.*, 2006, **124**, 034108.
61. C. J. Cramer, F. J. Dulles, D. J. Giesen, and J. Almlöf, *Chem. Phys. Lett.*, 1995, **245**, 165.
62. A. S. Menon, L. Radom, *J. Phys. Chem. A*, 2008, **112**, 13225.
63. N. J. Mayhall, K. Raghavachari, P. C. Redfern, L. A. Curtiss, and V. A. Rassolov, *J. Chem. Phys.*, 2008, **128**, 144122.
64. S. Goel and A. E. Masunov, *J. Chem. Phys.*, 2008, **129**, 214302.
65. V. A. Rassolov, J. A. Pople, M. A. Ratner, and T. L. Windus, *J. Chem. Phys.*, 1998, **109**, 1223.

Please note that the abstract and keywords will not be included in the printed book, but are required for the online presentation of this book which will be published on Wiley InterScience (www.interscience.wiley.com). If the abstract and keywords are not present below, please take this opportunity to add them now.

The abstract should be of short paragraph upto 100 words in length and keywords between 5 to 10 words.

Abstract: An overview of spin contamination and its relationship to broken-symmetry wave functions are presented. Spin operator expectation-value formulas are developed for use with generalized, unrestricted, and restricted spin orbitals. Current projection techniques are reviewed and illustrated for a variety of current theoretical methods.

Keywords: electronic structure; Hamiltonian; instability; molecular orbital; projection operators; single reference; spin; stability; symmetry breaking.